Spectroscopic Evidence for Ag(III) in Highly Oxidized Silver Films by X-ray Photoelectron Spectroscopy

Tiffany C. Kaspar,*,† Tim Droubay,† Scott A. Chambers,† and Paul S. Bagus‡

Pacific Northwest National Laboratory, P.O. Box 999, Richland, Washington 99354, United States, and Department of Chemistry, University of North Texas, 1155 Union Circle, # 305070, Denton, Texas 76203-5017, United States

Received: August 20, 2010; Revised Manuscript Received: October 12, 2010

In situ X-ray photoelectron spectroscopy (XPS) was utilized to identify the chemical state of silver in a range of silver oxide thin films obtained by codeposition of silver and atomic oxygen. A highly oxidized silver species was observed at an unexpectedly low Ag $3d_{5/2}$ binding energy (BE) of 366.8 eV with an associated broad satellite at 368.2 eV; this species was assigned as Ag(III). It was found to be highly unstable in vacuum but could be regenerated by further exposure to atomic oxygen. Both BE shifts and intensity changes of the O 1s peak were found to correlate with changes in the silver oxidation state. The theoretical XPS spectrum of high spin Ag(III) was calculated for both an isolated cation and an embedded AgO_6 cluster.

1. Introduction

For decades, it has been a goal to elucidate the mechanisms behind the unique chemistry of both oxygen-exposed silver metal and silver oxides. O-saturated silver metal supported on alumina is an effective partial oxidation catalyst that is extensively utilized in industrially important reactions such as the epoxidation of ethene[1−3] and the conversion of methanol to formaldehyde.[4] More recent investigations have explored further applications of silver catalysts, such as the epoxidation of propene to propene oxide[1] and the reduction of NO_x in lean-burn internal combustion engines.[5] Silver and silver oxides are also of interest in various electrochemical processes, for example as the catalytic cathode material[6] or as a component of fast ion conduction glasses that can serve as a solid state electrolyte.[7] Nanoparticle silver has been studied for catalytic and electrochemical processes,[8] as well as its antimicrobial properties.[9] Silver oxides have potential application in electrical, optical, and magneto-optical data storage devices,[10] as transparent conducting oxides,[11] and as a surface-enhanced Raman spectroscopy (SERS)-active substrate.[12] Determining the chemical state of both silver and oxygen is critical to developing a mechanistic understanding of the remarkable properties of these materials.

1.1. Silver Oxides. Silver metal exhibits unique oxidation properties: when exposed to O_2 at moderate temperatures and pressures, silver dissociatively adsorbs oxygen but does not form a bulk oxide.[2,3] The Ag−O bonds are strong enough to be stable but weak enough to allow catalytic chemistry to occur.[2,3] While silver does not oxidize in O_2 at room temperature, it will oxidize when exposed to ozone,[13,14] atomic oxygen,[15] or hyperthermal atomic oxygen (∼5 eV), which simulates conditions in low Earth orbit.[16,17] Oxidized silver can also be produced by electrochemical or wet chemical routes.[12,18] Silver oxides show atypical properties compared to 3d transition metal oxides, such as a propensity for Ag cation clustering with unusually short Ag−Ag distances, which can be near that of (or even shorter than) Ag metal.[19] This clustering is suspected of playing a role in subvalent silver compounds such as $[Ag_6]^{4+}[Ag^+]_4(SiO_4^{4-})_2$.[19] In early work, Orgel[20] proposed that there was substantial covalent Ag−O bonding character in silver oxides and that this bonding would favor the low coordination numbers and low spin features observed for these oxides. This analysis is a further indication of the unique and complex properties of these oxides, which is also hinted at in more modern theoretical treatments of the electronic structure of Ag_2O[21,22] and AgO.[23]

Ag_2O is a p-type transparent semiconductor that has the same cubic cuprite structure as Cu_2O, where the O anions form a bcc lattice and the Ag(I) cations are tetrahedrally coordinated,[21,22] as summarized in Table 1. The Ag−O bond length in Ag_2O is 2.052 Å.[22] In contrast, AgO crystallizes in a monoclinic structure distinct from that of CuO and is reported to be an n-type semiconductor.[24] Neutron diffraction has identified two distinct silver sites in the AgO lattice: Ag1 which is linearly coordinated by two O at a distance of 2.176 Å, and Ag2 which is approximately square planar coordinated by four O, two at a distance of 2.010 Å and two at 2.053 Å.[25] The lack of antiferromagnetic ordering observed by neutron diffraction implies that Ag(II) with an unpaired electron is not present; thus, linearly coordinated Ag1 was assigned to Ag(I) and square-planar-coordinated Ag2 was assigned to low spin Ag(III).[25] While mixed valence Cu(I) and Cu(III) is not observed in CuO, mixed-valence Au(I) and Au(III) in gold compounds is quite common.[22] To emphasize its mixed-valence nature, AgO is sometimes referred to as Ag_2O_2.

Although Ag_2O is stable indefinitely at room temperature in air, it decomposes at 450−700 K;[4,13,14,26,27] AgO decomposes to Ag_2O at 400−500 K.[14,26,28] Because the oxygen dissociation pressure of AgO is orders of magnitude higher than that of Ag_2O, it has been predicted[22] that AgO would not be stable in ultrahigh vacuum (UHV) conditions. Both oxides react with ambient CO_2 to form surface carbonate species.[14,27]

Silver can also form the higher oxidation state compounds Ag_3O_4 and Ag_2O_3. Ag_3O_4 crystallizes in a monoclinic structure with both Ag(II) and Ag(III) 4-fold coordinated by O; unusually, the Ag(II)−O bond distance (2.03 Å) is slightly shorter than the Ag(III)−O distance (2.07 Å).[14] Ag_3O_4 exhibits metallic

* To whom correspondence should be addressed. E-mail: tiffany.kaspar@pnl.gov.
† Pacific Northwest National Laboratory.
‡ University of North Texas.

10.1021/jp107914e
Published on Web 11/11/2010

TABLE 1: Summary of Structural Parameters and XPS BE Assignments for Silver Metal and Various Silver Oxides

	Ag metal	Ag_2O	AgO	Ag_3O_4	Ag_2O_3
structure	fcc	cubic cuprite[a]	monoclinic[b]	monoclinic[c]	square planar[c]
Ag charge state	Ag(0)	Ag(I)	1 × Ag(I) 1 × Ag(III)	1 × Ag(II) 2 × Ag(III)	Ag(III)
NN distance	2.89 Å	2.052 Å	Ag(I)−O: 2.176 Å Ag(III)−O: 2.010 and 2.053 Å	Ag(II)−O: 2.03 Å Ag(III)−O: 2.07 Å	2.02 Å average
BE Ag $3d_{5/2}$ (previous work)	368.1 ± 0.1 eV[d] 368.26 eV[e]	367.7 ± 0.1 eV[f]	367.3 ± 0.1 eV[g]	thermal instability[c]	
BE Ag $3d_{5/2}$ [fwhm] (this work)	368.24 eV [0.63 eV]	367.3 eV [1.1 eV] (367.5−367.7 eV for $Ag_2O_{1-\delta}$)	Ag(III): 366.8 eV [0.8 eV] + 368.2 eV [1.2 eV] satellite		
BE O 1s (previous work)		529.0 ± 0.2 eV[f]	528.5 ± 0.1 eV[g]		
BE O 1s [fwhm] (this work)		529.0 eV [0.8 − 1.2 eV]	528.4 eV [0.8 eV]		

[a] Tjeng et al.[22] [b] Scatturin and Bellon.[25] [c] Waterhouse et al.[29] [d] Schon.[26] [e] Moulder et al.[48] [f] Hoflund et al.[32] [g] Hoflund et al.[33]

conductivity.[29] Ag_2O_3 is isostructural with Au_2O_3, consisting of square-planar AgO_4 linked by common oxygens in a three-dimensional network; the average Ag(III)−O bond length is 2.02 Å.[29] Both oxides are very unstable. Ag_2O_3 is reported to decompose to AgO at room temperature in 1 h; Ag_3O_4 decomposes at 375 K.[14] Silver is not known to take the Ag(IV) valence.

Despite years of intensive effort, particularly regarding the catalytic epoxidation of ethene, the chemistry of the silver−oxygen system is not well understood. Much work has been devoted to determining the "active" adsorbed oxygen species that participates in partial oxidation reactions on silver, but no species has been conclusively proven responsible.[2,4,30] It has recently been suggested that O_2 dissociatively adsorbed as atomic oxygen forms a surface oxide consisting of ionic or nucleophilic oxygen and $Ag^{\delta+}$ species, which promote the adsorption and reaction of ethene.[31]

1.2. X-ray Photoelectron Spectroscopy of Silver Oxides. To better understand issues as varied as the mechanism of ethene epoxidation and the antimicrobial properties of silver nanoparticles, it is necessary to determine the chemical state of both silver and oxygen. X-ray photoelectron spectroscopy (XPS) provides a sensitive measure of the chemical state in the near-surface region of materials, and to this end XPS has been applied numerous times to silver and silver oxide systems. In 1973, Schon[26] reported the XPS spectra of Ag_2O and AgO powders, as well as clean Ag foil. He confirmed previous assignments of the binding energy (BE) of the Ag $3d_{5/2}$ peak from Ag(0) at 368.1 ± 0.1 eV. The Ag $3d_{5/2}$ peak position of Ag(I) in Ag_2O powder was found to shift to *lower* BE than that of Ag(0), with BE = 367.7 ± 0.2 eV. This negative BE shift is in contrast to the typical positive core level BE shifts of metal cations in ionic materials. The BE of the Ag $3d_{5/2}$ peak in AgO was further negatively shifted to 367.4 ± 0.2 eV, with a broadened full width at half-maximum (fwhm) that was attributed to the mixed valence Ag(I) and Ag(III) present in AgO. The O 1s peak position for Ag_2O was found to be 529.0 ± 0.2 eV, while the O 1s peak for AgO was shifted to 528.4 ± 0.2 eV. More modern studies on Ag_2O and AgO powders[27,28] have not altered these BE assignments in any substantial way, and thus they have become the accepted values within the XPS community[32,33] and are summarized in Table 1. Waterhouse et al.[29] attempted to record XPS spectra of freshly synthesized Ag_3O_4 but were unsuccessful due to the thermal instability of the compound.

The silver/silver oxide system was the first reported negative BE shift of metal cations with increasing oxidation,[26] although the phenomena was later observed in other systems such as cobalt, where Co(III) exhibits a lower BE than Co(II),[34] and barium, where Ba(II) in BaO shifts to lower BE than Ba(0).[35] Oxidation of a metal typically results in chemical shifts to higher BE for core electrons due to lower valence electron charge density.[28] For the silver/silver oxide system, the exact mechanism that results in negative BE shifts has not been elucidated, although in the original report Schon[26] emphasized that BE shifts are determined primarily by the Hartree potential; it has since been attributed to final state relaxation effects[29] and/or work function changes.[27] In the alkaline earth oxides, the negative BE shift for BaO was shown to arise from competition between the offsetting effects of chemical shifts due to charge on the cation (which acts to increase the BE) and the Madelung potential of the surrounding crystal lattice (which acts to decrease the BE).[35]

One significant drawback to utilizing silver oxide powders for XPS analysis is the inability to remove the substantial quantities of adventitious carbon and carbonate species present. Silver oxides decompose upon heating before all the contamination can be removed.[27,28] The presence of this surface layer complicates interpretation of the O 1s XPS spectra since several additional peaks due to carbonates and other contaminants are introduced and may impact the Ag 3d spectra as well. In situ reaction and XPS measurements can overcome this limitation. The first in situ work involved surface science studies of single crystal silver metal surfaces exposed to O_2 under various conditions in an effort to elucidate the mechanism(s) of partial oxidation catalysis. In general, these studies focused on the oxygen species present, and thus the O 1s XPS spectra; little if any shift in the Ag 3d spectra was observed under UHV conditions.[2,4]

It has long been known that exposing metallic silver to a strongly oxidizing species such as ozone or atomic oxygen results in bulk oxidation at room temperature.[36] Exposure of bulk silver metal to an oxygen plasma[22,24] or ozone[14] results in XPS spectra consistent with the Ag_2O peak assignments given in Table 1. Prolonged exposure to ozone at atmospheric pressure led to surface AgO formation, as evidenced by shifts in the Ag 3d and O 1s spectra.[14] Bielmann et al.[24] found that after exposure of single crystal silver to an electron cyclotron resonance (ECR) oxygen plasma source at room temperature to form Ag_2O, a second, intense O 1s peak was observed at 531.7 eV, which was attributed by the authors to the presence of O^- in AgO on the basis of theoretical calculations by Park et al.[23] In all these cases, the reported Ag $3d_{5/2}$ peak positions are within ±0.1 eV of the accepted values[27,28] for Ag(I) and Ag(III). In a recent study, Lutzenkirchen-Hecht et al.[18] electrochemically oxidized polycrystalline silver foil to AgO and confirmed the structure with in situ extended X-ray absorption fine structure (EXAFS). Ex situ XPS revealed a broad Ag $3d_{5/2}$ peak that was fit with two primary peaks located at 367.25 and 367.97 eV. This was interpreted as further evidence of the mixed valence nature of AgO. Substantial oxygen substoichiometry (up to 30%) was observed in AgO, primarily around the Ag(III) cations, without a structural change in the AgO crystal, as measured by EXAFS.

XPS of silver clathrate salts (formally $(Ag^{2+})_2(Ag^{3+})_4O_8Ag^{1+}X^-$, where X is a salt) resulted in a broad Ag $3d_{5/2}$ peak located at 367.4 eV,[4,29] which is unexpectedly consistent with the peak position assignment in AgO despite the additional presence of Ag(I) in AgO versus Ag(II) in the clathrate. A satellite in the Ag $3d_{5/2}$ peak was observed at a low BE of ~366.0 eV,[4,29] attributed to final state effects in the clathrate compound.[4]

The deposition of silver oxide thin films for the purpose of obtaining XPS spectra is much less common. Thin film deposition (or oxidation of a thin silver metal film) has the advantage of potentially achieving much more highly oxidizing conditions compared to oxidation of a bulk silver foil, since silver metal can act as a substantial sink for oxygen. Silver oxide films have been deposited by sputtering,[10,37] pulsed laser deposition,[9] and electrodeposition.[12] Rivers et al.[11] deposited silver metal in the presence of an ECR oxygen plasma on Al_2O_3 substrates to obtain oxidized thin films; however, since the goal was to obtain phase-pure Ag_2O films, very highly oxidizing conditions were not explored.

The relatively small BE shifts with oxidation state of the Ag 3d peaks makes it difficult to confirm the silver oxidation state, particularly on samples that have been contaminated by atmospheric exposure.[11,28,38] Some groups have attempted to utilize the Ag MNN Auger peaks to quantify the oxidation state of silver; these peaks change line shape dramatically as silver oxidizes, although the small quantitative shifts between Ag metal, Ag_2O, and AgO make it difficult to determine the silver charge state from the Auger peaks alone.[11,14,28] Similarly, the O 1s peak has been investigated as a measure of oxidation state in silver oxides. While the peak shift between Ag_2O and AgO appears to be reproducible,[26−28] the O 1s spectrum also frequently contains contributions at higher BE, which have been attributed variously to hydroxyls, carbonates, subsurface O, or lattice O in AgO (see Bao et al.[4] for a detailed discussion).

The current work represents a significant extension of these previous XPS studies by reporting in situ XPS spectra of highly oxidized silver films, which have been codeposited in the presence of atomic oxygen to achieve a range of silver oxidation states. Under moderately oxidizing deposition conditions, Ag $3d_{5/2}$ peaks at the positions described above for Ag_2O and AgO were obtained. However, under very highly oxidizing conditions, a new peak appeared in the Ag 3d spectra at lower BE (366.8 eV for Ag $3d_{5/2}$) than previously reported; a satellite peak at higher BE (368.2 eV) was associated with this feature. Considering the chemistry of silver, this peak and satellite are assigned to low spin Ag(III). This result calls into question the previous spectral assignments for Ag(I) and Ag(III) accepted in the literature.

2. Methods

2.1. Silver Oxide Film Deposition. All silver samples were prepared in a molecular beam epitaxy (MBE) chamber with a working base pressure of 2×10^{-8} Torr. Silver films were deposited from an electron beam evaporator. The silver deposition flux was calibrated with a quartz crystal microbalance (QCM) placed in the sample position; flux control during deposition was provided by atomic absorption (AA) spectroscopy with feedback control to the electron beam evaporator. For "fast" silver depositions, the silver flux on the sample was $(0.5-1.1) \times 10^{14}$ Ag atoms/(cm^2·s) (equivalent to 0.09−0.19 Å Ag metal/s), while for "slow" depositions the flux was reduced to 6×10^{12} Ag atoms/(cm^2·s) (0.01 Å Ag metal/s). Total film thicknesses cannot be estimated since the oxide phase cannot be well established, but depositions were stopped after the equivalent of 25−100 Å of silver metal was deposited; these equivalent thicknesses will be reported below. Oxygen was supplied from an electron cyclotron resonance (ECR) microwave plasma source that provides a flux[39] of approximately 8×10^{12} to 4×10^{13} O atoms/(cm^2·s) at 25−40 mA applied magnetron current, with little contribution from O ions. Substrates were polycrystalline Au-coated quartz QCM crystals mounted on a conventional sample holder. All depositions and post-growth plasma soaks were performed at room temperature.

In situ XPS measurements utilizing monochromatized Al Kα X-rays ($\lambda = 1486.6$ eV) were obtained in an appended analytical chamber. The GammaData/Scienta SES-200 spectrometer provides high energy resolution (approximately 0.5 eV). All spectra were collected at normal takeoff angle (90°) unless noted otherwise (the small acceptance angle of the spectrometer allows angle-resolved measurements at takeoff angles down to ~8°). The semiconducting nature of silver oxides, as well as deposition on gold films, ensured that there was no charging during XPS measurements. Gold also provided an in situ binding energy reference; the Au $4f_{7/2}$ peak position at 84.0 eV was confirmed for each sample. Peaks were fit with symmetric Voigt (Gaussian * Lorentzian) peak shapes after subtraction of a Shirley background. As a spectral reference, a polycrystalline silver foil was sputtered clean and measured under the same conditions as the silver films.

2.2. Electronic Structure Calculations. We have carried out calculations of the electronic structure for the initial and the final, 3d core-ionized, states of the Ag(III) cation to predict the resultant photoemission spectra. We have included many-body terms arising from intra-atomic effects, which lead to multiplet splitting,[40,41] and from interatomic, or charge transfer (CT), effects.[41−44] The relative energies, E_{rel}, and relative intensities, I_{rel}, for the theoretical 3d XPS are then determined. Two material models were utilized for the silver oxides; one model is an isolated Ag(III) cation and the second model is an embedded cluster to model AgO that includes the interaction of the Ag cation with the surrounding O anions. In this work, we have assumed that the Ag(III) cation is in a high spin state. This assumption was made to test the possibility that the measured Ag XPS spectra for Ag(III) might include multiplet splitting effects that arise because there is an open 4d shell in the material; see Bagus et al.[41] and references therein. In later work, we will present models of low spin complexes. The procedure for the calculations follows that described in previous papers;[41,44] in the Supporting Information, section S1, we review the methodology used.

3. Results

Figure 1a shows a typical XPS survey spectrum of silver metal codeposited with atomic oxygen on an Au-coated QCM crystal; the film was soaked in the plasma for 2.5 h after the silver flux was stopped. Although the equivalent silver metal thickness deposited was approximately 100 Å, the underlying Au substrate is still clearly observed in the survey spectrum. This indicates that the oxidized silver film is discontinuous and likely exhibits island growth on the gold substrate;[45] island growth may be especially favored due to the roughness of the gold suface. Another possibility is that gold and silver have interdiffused to form an alloy,[46] although bulk diffusion through 100 Å of silver metal seems less likely at room temperature. The presence of gold under all deposition conditions implies that the valence band measured by XPS would be the complex combination of that from the silver oxide of interest and the underlying gold; for this reason, valence band spectra were not

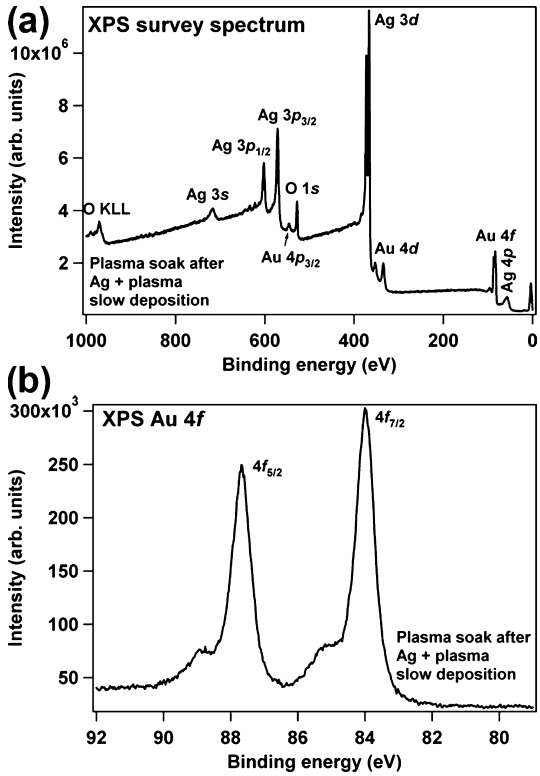

Figure 1. (a) XPS survey spectrum of a silver film codeposited with atomic oxygen on an Au-coated QCO crystal. The film was soaked in the plasma for 2.5 h after deposition. Ag, Au, and O photoemission and Auger peaks are labeled. (b) high resolution XPS spectrum of the Au 4f region for the same film. The shoulders present on the high binding-energy side of each peak indicate the formation of AuO_x.

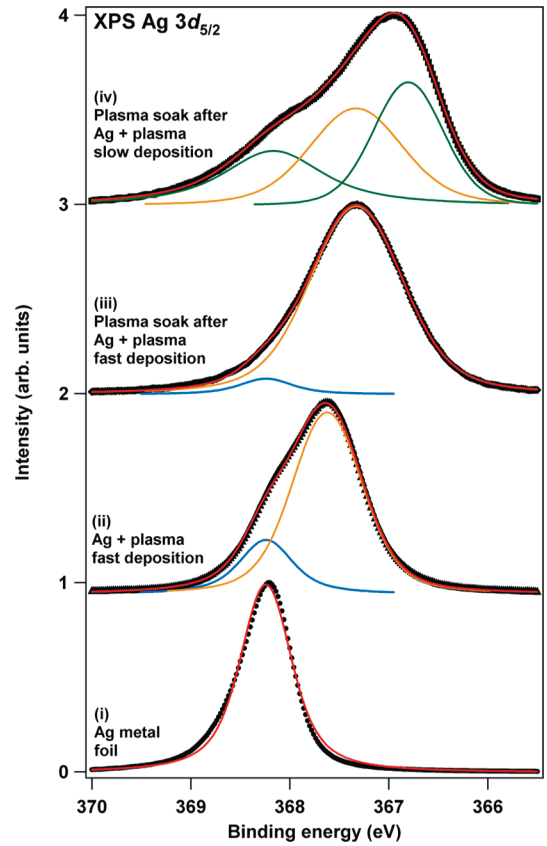

Figure 2. High resolution XPS data of the Ag $3d_{5/2}$ region (symbols) for polycrystalline silver foil, as well as oxidized silver films deposited with atomic oxygen under different conditions. Peak intensities are normalized. Fitted peaks (Voigt functions) are shown as thin solid lines; the fitted peak sums are shown as thick lines. Relevant fitted peak parameters are given in the text.

collected. The high BE shoulder on both the Au $4f_{7/2}$ and $4f_{5/2}$ peaks in Figure 1b indicates that the deposition and plasma soak conditions are sufficient to partially oxidize the underlying gold.

3.1. XPS Spectra with Increasing Silver Oxidation. The evolution of the Ag $3d_{5/2}$ core-level peak with increasingly oxidative conditions is illustrated in Figure 2. As a reference, the spectrum of sputter-cleaned silver foil is included (Figure 2i). Since the peak for Ag(0) shows asymmetry on the high BE side characteristic of metals with a high density of states near the Fermi level (resulting in a large population of low lying final states), the best fit to the peak would be achieved by convolving a Gaussian function with an asymmetric Doniach−Sunjic function.[47] However, it was found that the peak could be fit reasonably well with a symmetric Voigt function centered at 368.24 eV with a fwhm of 0.63 eV, which is sufficient for the purposes of this work. This peak position is in excellent agreement with the reference value of 368.26 eV.[48]

It is well established that silver does not oxidize in the presence of molecular O_2 at room temperature,[49] and we have previously confirmed that no oxidation occurs in molecular O_2 under our deposition conditions.[39] To achieve varying levels of silver oxidation, both the silver deposition flux and the atomic oxygen flux from the ECR plasma source were varied. Under "fast" deposition conditions (0.19 Å Ag metal/s), the maximum atomic oxygen flux produced in the ECR plasma is insufficient to fully oxidize the incoming silver, resulting in a mixed-phase thin film consisting of both silver metal and oxidized silver. The XPS Ag $3d_{5/2}$ spectrum (Figure 2ii) can be fit with two peaks, one with parameters held at the position and shape for Ag(0), and the other centered at 367.62 eV (fwhm = 0.83 eV). This position is in good agreement with previous assignments for Ag(I) in Ag_2O.[27] The presence of Ag_2O as the sole oxidized phase of silver is reasonable considering the mild oxidative conditions. The O 1s core level spectrum consists of two peaks, as shown in Figure 3ii. The peak at 528.91 eV (fwhm = 0.86 eV) is again consistent with Ag_2O,[27] and a higher BE contribution at 530.81 eV (fwhm = 1.58 eV) is clearly visible.

Silver deposition at 0.09 Å Ag metal/s with a lower flux of atomic oxygen resulted in virtually no silver oxidation in a 25 Å thick film (not shown); after soaking the film in a higher flux of atomic oxygen for 20 min, substantial silver oxidation occurred, as shown in Figure 2iii. The Ag $3d_{5/2}$ spectrum can again be fit with two peaks: one fixed to the parameters for Ag(0), and the second placed at 367.33 eV (fwhm = 1.11 eV). The accepted assignment for Ag $3d_{5/2}$ at this position is Ag(III) in AgO, although the measured fwhm is considerably narrower than that observed in previous work (for example, Weaver et al.[28] measured a fwhm of 1.75 eV, attributed to overlap of Ag(I) and Ag(III) peaks). The O 1s spectrum (Figure 3iii) again consists of two peaks: 529.04 eV (fwhm = 1.26 eV) and 530.38 eV (fwhm = 2.56 eV); previous work[28] has placed the O 1s BE for AgO at a lower BE value of 528.5 eV. The silver oxide film was found to be very stable with time, remaining virtually unchanged after storage for 3 months in UHV.

In an effort to obtain XPS data on pure AgO without the presence of residual Ag(0), a thicker film (100 Å) was deposited under slow conditions (0.01 Å Ag metal/s for a total deposition time of 2.75 h); after deposition ended, the film soaked in the oxygen plasma an additional 2.5 h. As shown in Figure 2iv, an unexpected Ag $3d_{5/2}$ peak shape resulted. Three peaks are

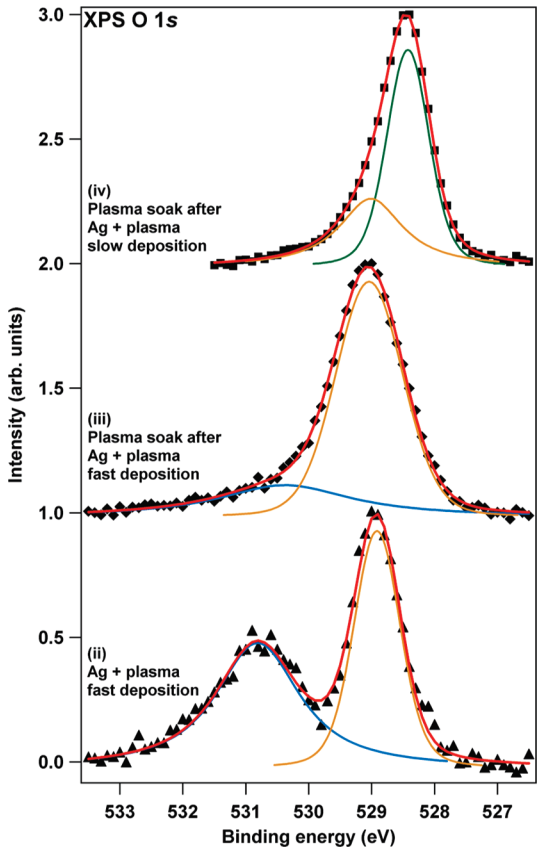

Figure 3. High resolution XPS data of the O 1s region (symbols) for oxidized silver films deposited with atomic oxygen under different conditions. Peak intensities are normalized. Fitted peaks (Voigt functions) are shown as thin solid lines; the fitted peak sums are shown as thick lines. Relevant fitted peak parameters are given in the text.

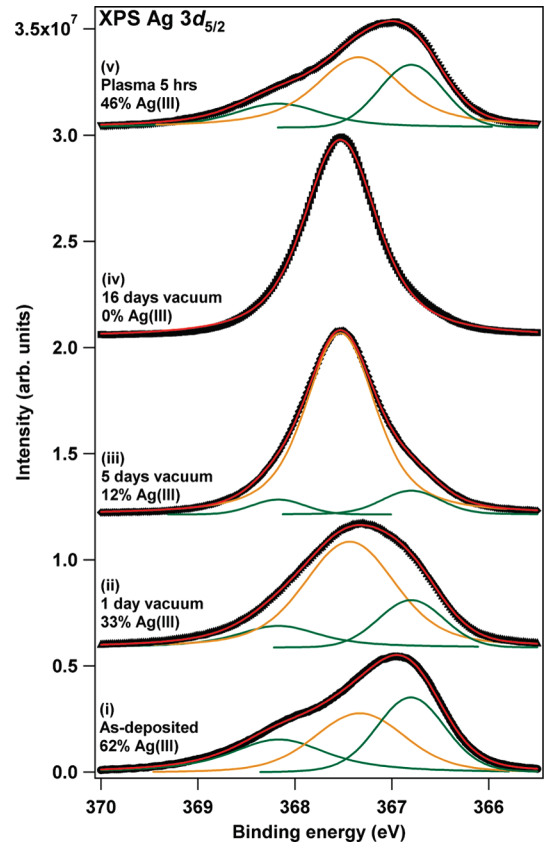

Figure 4. High resolution XPS data of the Ag $3d_{5/2}$ region (symbols) for an 100 Å silver film deposited with atomic oxygen under slow deposition conditions (0.01 Å Ag metal/s), followed by a soak in the oxygen plasma for 2.5 h. The as-deposited spectrum (bottom) was collected immediately after the plasma soak; subsequent spectra were collected after sitting in UHV for the specified time. After 19 days in UHV, the film was soaked in the oxygen plasma for 5 h. Peak intensities are not normalized. Fitted peaks (Voigt functions) are shown as thin solid lines; the fitted peak sums are shown as thick lines. Relevant fitted peak parameters are given in the text.

required to fit this manifold: 368.17 eV (fwhm = 1.19 eV), 367.33 eV (1.11 eV), and 366.80 eV (0.83 eV). Although the peak at 368.17 eV is at a BE consistent with Ag(0), this assignment is implausible for two reasons: first, the very highly oxidizing conditions experienced by the film makes unoxidized Ag(0) unlikely, and second, the fwhm of this peak is much wider than that of Ag(0); in contrast to the previous spectra, this manifold cannot be fit well if the 368.17 eV peak is restricted to the fwhm of Ag(0), 0.63 eV. While the peak at 367.33 eV is consistent with Ag(III) in AgO, the peak at 366.80 eV has not been reported previously. In the raw Ag $3d_{5/2}$ spectrum, the peak maximum occurs at 366.95 eV, indicating that the low BE for the primary peak component is not an artifact of peak fitting but instead represents a real BE shift. As discussed in detail below, we assign the peak at 366.80 eV to Ag(III), and the peak at 368.17 eV as a satellite of this peak.

Concurrent with the new spectral features in the Ag 3d peaks, a second lattice oxygen peak appears in the O 1s spectrum (Figure 3iv) at 528.42 eV (fwhm = 0.79 eV). This peak position is consistent with the O 1s position in AgO,[28] although in previous studies it occurred when the Ag $3d_{5/2}$ peak position was approximately 367.3 eV. A substantial contribution from a peak centered at 529.01 eV (fwhm = 1.22 eV) indicates that this oxide is a mixed-phase material, since all the known silver oxides consist of only one oxygen lattice position.

The Ag MNN spectra for each of the samples is given in the Supporting Information (section S2). It was found that the small and somewhat inconsistent Ag MNN peak shifts render it difficult to determine the silver oxidation state on the basis of the Ag MNN Auger spectra alone.

3.2. Properties of the Highly Oxidized Silver Species. The highly oxidized silver oxide species proved to be stable under reasonable X-ray exposure (a couple of hours), but very unstable with time during storage in UHV. The rapid decomposition of this oxide is illustrated in Figure 4 for the Ag $3d_{5/2}$ spectra and Figure 5 for the O 1s spectra. In the Ag $3d_{5/2}$ spectra of the film immediately following deposition and plasma soak (Figure 4i), the spectral features at 366.80 and 368.17 eV combined are 62% by area of the Ag $3d_{5/2}$ region. To fit subsequent spectra, the position and fwhm of these high oxidation state peaks were fixed, while the central Ag peak representing lower oxidation was allowed to vary position and fwhm. The intensities of the high oxidation state peaks both drop dramatically after 1 day in UHV (Figure 4ii). In the initial spectrum, the area ratio of the contribution at 366.80 eV to the satellite at 368.17 eV is 1.22; after sitting in UHV for 1 day, a similar ratio of 1.02 is obtained, although the contribution of these two peaks to the overall Ag $3d_{5/2}$ intensity has dropped from 62% to 33%. After 5 days in UHV the peaks have decreased further (Figure 4iii, 12% of Ag $3d_{5/2}$, area ratio of 2.00), and the central lower-oxidation peak has shifted from 367.33 to 367.53 eV. After 16 days in UHV (Figure 4iv) the high oxidation state peaks disappear completely, and the Ag $3d_{5/2}$ spectrum consists of only one species at 367.53 eV (fwhm = 0.96 eV). Exposure of this decomposed film to the ECR plasma for 5 h (approximately the same amount of time as the deposition plus plasma soak

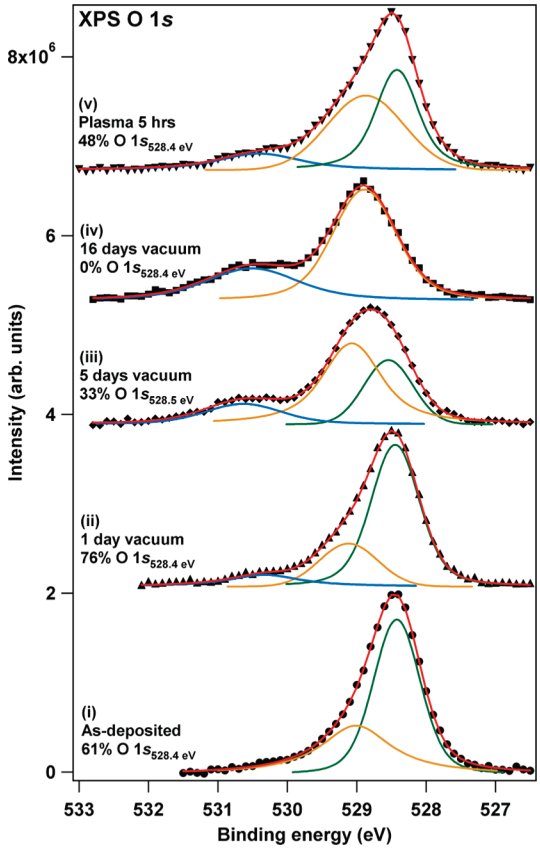

Figure 5. High resolution XPS data of the O 1s region (symbols) for an 100 Å silver film deposited with atomic oxygen under slow deposition conditions (0.01 Å Ag metal/s), followed by a soak in the oxygen plasma for 2.5 h. The as-deposited spectrum (bottom) was collected immediately after the plasma soak; subsequent spectra were collected after sitting in UHV for the specified time. After 19 days in UHV, the film was soaked in the oxygen plasma for 5 h. Peak intensities are not normalized. Fitted peaks (Voigt functions) are shown as thin solid lines; the fitted peak sums are shown as thick lines. Relevant fitted peak parameters are given in the text.

for the original film) results in reoxidation to a similar level as observed initially (Figure 4v). The peaks at 366.80 and 368.17 eV reappear, with an area ratio of 1.5. The central lower-oxidation peak also shifts position back to 367.34 eV.

Fairly similar decomposition behavior is observed for the 528.4 eV contribution to the O 1s spectrum, as shown in Figure 5. Immediately after deposition and plasma soak (Figure 5i), the 528.4 eV peak comprised 61% by area of the lattice oxygen (the high BE contribution at ~530.5 eV was not included). After 1 day in UHV, the contribution of the 528.4 eV peak to the lattice oxygen actually increased slightly, from 62% to 76% (Figure 5ii). However, after 5 days in UHV (Figure 5iii) the 528.4 eV contribution had dropped substantially, to 33% of the lattice oxygen. After 16 days in UHV (Figure 5iv), the peak at 528.4 eV disappeared completely, concurrent with the disappearance of the 366.8 and 368.2 eV peaks in the Ag $3d_{5/2}$ spectrum (Figure 4iv). After exposure to the ECR plasma for 5 h (Figure 5v), the peak at 528.4 eV reappears at nearly the same level as initially, comprising 48% of the lattice oxygen. These peak area changes with time are plotted quantitatively in Figure 7a for both the 528.4 eV contribution to the O 1s spectra and the Ag(III) contribution to the Ag $3d_{5/2}$ spectra.

3.3. Model Calculations of Ag 3d Spectra for High Spin Ag(III) Complexes. To aid in interpreting the charge state and satellite structure of the highly oxidized silver species shown

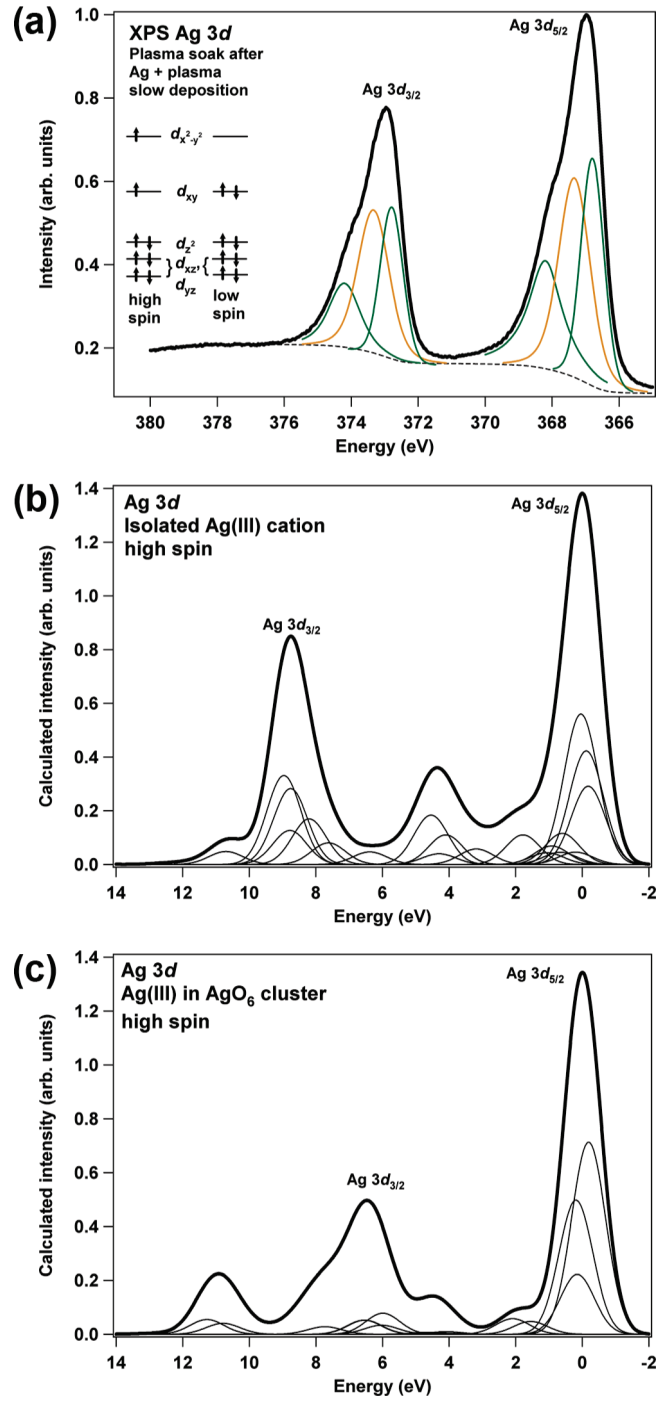

Figure 6. (a) High resolution Ag 3d spectrum (thick black line) of highly oxidized silver (also shown in Figure 2 top and Figure 4 bottom). Ag(III) contributions to the spectra are shown as green fitted peaks; Ag(I) contributions are yellow fitted peaks. The dotted line indicates the Shirley background utilized for peak fitting. (b) Calculated Ag 3d spectrum for the isolated Ag(III) cation in high spin configuration. Individual contributions are shown as thin lines; the thick line indicates their sum. (c) Calculated Ag 3d spectrum for high spin Ag(III) in an AgO_6 cluster. Individual contributions are shown as thin lines; the thick line indicates their sum.

in Figure 2iv, and reproduced with both Ag $3d_{5/2}$ and Ag $3d_{3/2}$ contributions in Figure 6a, theoretical calculations of the Ag 3d spectra of high spin Ag(III) complexes were performed. For clarity, the expected energy level diagram and electron configurations for high spin and low spin d^8 cations in an undistorted square planar crystal field[50] are illustrated in Figure 6a. The theoretical spectra for a high spin isolated Ag(III) cation is

shown in Figure 6b, where individual important contributions as well as the envelope summing the contributions are shown. The "spin orbit" splitting of Ag $3d_{5/2}$ and $3d_{3/2}$ is approximately 2 eV larger in the calculation than the tabulated experimental value[48] (~8 eV versus 6.00 eV) because the splitting of the XPS peaks for $j = l + 1/2$ and $j = l - 1/2$ core levels is strongly influenced by chemical bonding[41] as well as by many-body effects. Clearly, neither covalent bonding nor CT many-body effects are included in the isolated Ag(III) calculation, and thus the discrepancy between the calculated and measured spin−orbit splittings is not surprising. The first calculated peak at $E_{rel} = 0$ eV is composed of several different multiplet split peaks that result in a relatively narrow main peak (corresponding to $3d_{5/2}$) and a weak satellite at $E_{rel} \approx 2.0$ eV. This satellite peak is at too high an energy and has too low intensity to correspond to the 368.2 eV satellite, $E_{rel} = 1.4$ eV, observed in the XPS measurements. The satellite at $E_{rel} \approx 4.5$ eV is composed of approximately equal contributions from $3d_{3/2}$ and $3d_{5/2}$ ionization. The experiment shows no indication of this 4.5 eV satellite in Figure 6a. Thus, on the basis of the generalized multiplets for the isolated Ag(III) cation, we would conclude that the XPS observed and assigned to Ag(III) does not arise from a high spin Ag(III) cation. This conclusion is further confirmed when we examine the theoretical 3d spectrum for the high spin embedded AgO_6 cluster shown in Figure 6c. In this case the multiplets in the main peak have a somewhat smaller splitting, although the fwhm of approximately 1.3 eV is still considerably broader than the 366.8 eV contribution to the experimental Ag $3d_{5/2}$ spectrum (fwhm = 0.83 eV). The weak satellite at ~2 eV has somewhat less relative intensity than the calculation for the isolated cation and moves to a slightly higher E_{rel}. Again, it is not possible to associate this weak satellite with the observed XPS satellite at $E_{rel} = 1.4$ eV. The intensities and structure of the satellite at $E_{rel} \approx 4$ eV and the $3d_{3/2}$ XPS peak now at ~7 eV are changed and broadened significantly due to the inclusion of CT configurations, and a new satellite at $E_{rel} \sim 11$ eV appears, none of which is consistent with the experimental XPS spectra. The overall conclusion is that the observed XPS are consistent with a low spin Ag(III) cation rather than a high spin cation. The role of CT configurations, and of shake configuration, for low spin Ag(III) will be presented for more realistic, low symmetry, cluster models of A(III) cations in AgO in future work.

4. Discussion

4.1. Mechanism of Negative BE Shift for Silver Oxides. The observed negative BE shift with increasing oxidation for the closed-shell Ag(I) cation can be understood as a result of two competing effects: the chemical shift due to charge on the cation, and the Madelung potential due to the crystalline environment.[35,51] Removing an outer shell electron, in this case the $Ag(5s^1)$, to leave a closed shell cation always leads to an increase in the BE. However, this increase is smaller as the orbital of the removed electron becomes larger or more diffuse. To a first approximation, $\Delta BE \propto + 1/\langle r \rangle_{ns}$ where $\langle r \rangle_{ns}$ is the mean value of the orbital radius of the ns electron removed when the cation is formed. Thus, for example, removing the more compact Cu(4s) orbital leads to a greater shift to higher BE than does removing the more diffuse Ag(5s) orbital. However, the electrostatic potential due to the charges on the surrounding ions in an ionic crystal, the Madelung potential, also shifts the cation BE's. In all cases, the sign of the Madelung potential at a cation site is negative, which shifts the cation BE's to smaller values. The magnitude of this shift will be inversely proportional to the metal−oxygen distance, becoming larger as the lattice constant becomes smaller. In the case of Ag_2O, the magnitude of the Madelung potential may dominate over the positive chemical shift, resulting in an overall negative BE shift. Silver compounds are known to possess unusually short bond lengths;[19] the Ag−O bond length[22] in cuprite Ag_2O is 2.05 Å while for comparison the Mn−O distance in MnO is almost 10% larger at 2.22 Å. This is consistent with the core level BE shifts for Mn in MnO being positive relative to Mn(0) and the Ag core level shifts in silver oxides being negative relative to Ag(0). A similar effect may also occur for the O 1s BE, although in this case the additional electron on the O^- anion results in a negative chemical shift while the Madelung potential acts to increase the BE. However, to fully understand the exact trade-off between the Madelung potential and chemical shift in silver oxides, including the effects of covalency[41,52] in the Ag−O bonding, requires further theoretical study.

4.2. Assignment of Ag $3d_{5/2}$ 366.8 and 368.2 eV to Ag(III). With the accepted assignment of Ag $3d_{5/2}$ at 367.4 eV to Ag(III) in AgO,[28] the observation shown in Figure 2iv of substantial spectral intensity at a lower BE of 366.8 eV is difficult to interpret. Assuming that higher oxidation state silver species continue the trend of shifting to lower BE with oxidation, this peak could be assigned to Ag(IV); however, no Ag(IV) species are known. Another possibility is that the peak is due to Ag(II), which is not present in AgO but is a constituent (along with Ag(III)) of the higher oxidation compound Ag_3O_4. This assignment would require Ag(II) to have an anomalously large negative shift, which places it at lower BE than Ag(III). However, Ag_3O_4 consists of twice as many Ag(III) as Ag(II), which is not consistent with the nearly equal peak areas of the species shown in Figure 2.

On the basis of the above experimental and theoretical arguments, we assign the Ag $3d_{5/2}$ peak at 366.8 eV to core-level photoemission from Ag(III), and the peak at 368.2 eV as a satellite of Ag(III) core-level photoemission. As discussed above, the peak at 368.2 eV could not be fit with the narrow fwhm expected for Ag(0), identifying this peak as originating from oxidized, not metallic, silver. The core-level and satellite peaks are clearly linked, as evidenced by their concurrent disappearance and reappearance with decomposition and reoxidation, respectively. The peak area ratio of 366.8−368.2 eV remains in the range 1.0−2.0 during the time series presented in Figure 4. As shown in the Supporting Information, section S3, the peaks maintain this ratio when the XPS takeoff angle is changed from 90° (more bulk-sensitive) to 12° (more surface sensitive), further confirming that the two peaks arise from the same species.

Unfortunately, the oxide stoichiometries of the spectra presented in Figures 2−5 could not be successfully calculated from the Ag 3d and O 1s peak areas, even when XPS cross sections and the appropriate Scienta spectrometer transmission function corrections were applied. In all cases, the stoichiometries were calculated to be severely oxygen-poor. For example, the highly oxidized film presented in Figures 2iv and 3iv and again in Figures 4i and 5i is expected to possess a stoichiometry equivalent to that of AgO (Ag/O = 1) or a higher oxide (Ag/O < 1). However, using Scofield photoionization cross sections[53] or the photoionization cross sections from Yeh and Lindau[54] and applying the Scienta transmission function, the Ag 3d/O 1s ratio is 2.8; using the experimental sensitivity factors determined by Wagner[55] and the same transmission function, the ratio is 3.7. In no case for the films presented above could an Ag/O ratio of 2.0 or less (in Ag_2O, Ag/O = 2) be obtained by any calculation. This discrepancy in the calculated Ag/O

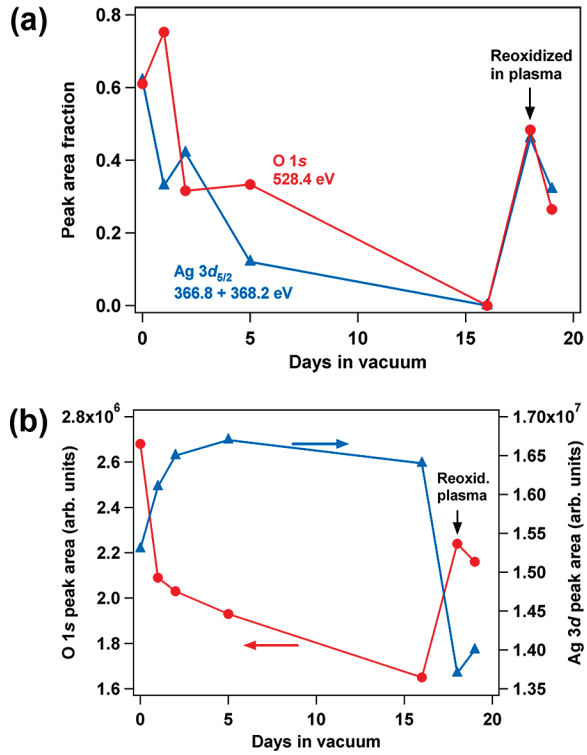

Figure 7. High resolution XPS spectral fitting data taken from Figures 4 and 5. For all spectra, the O 1s high BE contribution was not included. (a) Peak area fractions of the total lattice O 1s spectrum fitted by a peak at 528.4 eV, and of the total Ag $3d_{5/2}$ spectrum fitted by peaks at 366.8 and 368.2 eV. (b) Total lattice O 1s and Ag 3d peak areas, determined from XPS survey spectra.

ratios compared to the expected values has been previously observed, and attributed to either inaccurate photoionization cross sections[4] or substantial oxygen substoichiometry in silver oxides.[18] As discussed further below, an additional contribution to this discrepancy may be that the intensity lost to shake satellites may depend strongly on the species, environment, and chemical bonding of the core ionized atom.

Further insight may be gained by investigating the total O 1s and Ag 3d peak areas during the oxide decomposition and reoxidation series presented in Figures 4 and 5. As plotted in Figure 7b, the O 1s peak area due to lattice oxygen is maximum for the film immediately after deposition and plasma soak. As the film sits in UHV, the lattice O 1s peak area decreases, indicating oxygen loss from the oxide. After exposure to the plasma, the lattice O 1s peak area again increases, as expected if the plasma treatment is reoxidizing the silver oxide decomposition species. However, changes in the Ag 3d peak area are more difficult to interpret. Nominally, oxidation and reduction of the silver species would not be expected to cause a change in the total Ag 3d peak area, since no silver atoms are being gained or lost from the system. However, Figure 7b shows that the Ag 3d peak area is a minimum for the fully oxidized film; as the oxide decomposes, the Ag 3d area increases concurrent with the decrease of the lattice O1s peak area. When the film is again exposed to the plasma, the Ag 3d peak area again decreases. It is unlikely that the peak area changes are due to density changes in the various silver oxides; the change in number density of silver cations between AgO and Ag_2O is less than 3%, while in Figure 7b the Ag 3d peak area decreases by ~20% after reoxidation of the decomposed film. Etching or sputtering of the oxidized silver film by the oxygen plasma is not expected and can be ruled out by the Au 4f peak of the underlying gold, which shows no increase after exposure of the oxidized silver film to the oxygen plasma for 5 h. One potential explanation for the decrease in Ag 3d peak area with plasma exposure is that there is a very large difference in the shake satellite probabilities between Ag 3d and O 1s, as well as between Ag 3d in various oxidation states, in silver oxides with some degree of covalent bonding. Shake satellites can occur far from the core-level peaks and be barely detectable above background; spectral intensity is "lost" from the core-level peak and transferred to these features.[44] This effect may explain both the anomalous Ag 3d peak area changes with oxidation, as well as the discrepancies in the calculated Ag/O stoichiometry discussed above. Changes in shake satellite probability imply that the photoionization cross sections determined for the pure materials cannot be applied to the oxide. However, without independent measurements of the silver and oxygen content of these films, oxygen substoichiometry cannot be ruled out.

4.3. Assignment of Ag $3d_{5/2}$ 367.3−367.7 eV to Ag(I). It is obvious that, if the Ag $3d_{5/2}$ peak at 366.8 eV is assigned to Ag(III), the peak at 367.3 eV, previously assigned to Ag(III),[28] must be revisited. The two likely silver oxidation states are Ag(I) and Ag(II). However, in contrast to previous studies that have reported a wide fwhm of 1.7−1.9 eV for this peak,[14,26,28] it has been obtained in the present study with a relatively narrow fwhm of 1.11 eV (Figure 2iii). This relatively narrow peak width indicates that the peak originates from a single silver oxidation state, not a mixed-valence oxide, as suspected previously. Since there are no known silver oxide phases that consist exclusively of Ag(II), we assign the Ag $3d_{5/2}$ peak at 367.3 eV to Ag(I). In the course of the present study, this peak has been observed to shift from 367.3 to 367.5 eV (Figure 4) and to appear at 367.6 eV (Figure 2ii). This large of a BE shift for a single oxidation state in different oxide compounds would be considered unusual; instead, the shift is attributed to the ease with which silver compounds form substoichiometric species,[19] which appear to maintain the bulk crystal structure.[18,29] Hence, 367.3 eV is assigned as the BE position for fully stoichiometric Ag(I), while the shifts to higher BE represent $Ag^{1-\delta}$ stoichiometries, where δ represents the oxygen substoichiometry of the $Ag_2O_{1-\delta}$ compound. As discussed above, the Ag/O stoichiometry for these materials cannot be calculated quantitatively, but the raw Ag/O peak area ratio of 13.4 for fully stoichiometric Ag_2O (367.3 eV, Figure 2iii) is substantially lower than that for substoichiometric Ag_2O, 16.7 (367.7 eV, Figure 2ii), indicating qualitatively that more oxygen is present in the compound with a lower Ag $3d_{5/2}$ BE. The Ag $3d_{5/2}$ peak is also found at 367.3 eV for powders and films that have been confirmed by structural analysis to possess the AgO crystal structure. Since AgO has been predicted to be unstable in vacuum[22] and substoichiometry in AgO has been found to primarily affect the Ag(III) species,[18] we speculate that the peak previously assigned to Ag(III) actually arises from Ag(I) decomposition products.

It should be noted that another possibility for the discrepancy between the current results and previous studies is that the present study provides evidence that AgO consists of Ag(II), not mixed valence Ag(I) and Ag(III), and thus the Ag $3d_{5/2}$ spectrum for pure, stoichiometric AgO consists of a single Ag(II) peak at 367.3 eV. Further oxidation results in metastable Ag_3O_4, with the Ag(II) peak at 367.3 eV still present and additional peaks at 366.8 and 368.2 eV due to Ag(III). However, this is not very likely, since it has been confirmed by several techniques[18,25] that the AgO crystal structure possesses two distinct lattice sites for silver, and no magnetic evidence for Ag(II) with an unpaired electron has been reported. Electronic

structure calculations by Park et al.[23] predicted that AgO would consist of Ag(I) and Ag(II), with oxygen holes (O^-) present to maintain charge neutrality. However, in this model AgO consists of equal amounts of Ag(I) and Ag(II), which does not support the observation of a narrow peak at 367.3 eV likely arising from a single oxidation state.

4.4. Assignment of O 1s 528.4 eV to AgO. As illustrated in Figure 7a, the O 1s contribution at 528.4 eV rises and falls with Ag(III) in the Ag $3d_{5/2}$ spectrum, providing a strong indication that these species are correlated. From this, we assign the O 1s peak at 528.4 eV to oxygen in AgO. In contrast to the Ag(III) peak discussed above, the O 1s peak at 528.4 eV for AgO has been observed many times previously, including in AgO powder samples.[26,28] As discussed in the Supporting Information, section S3, the presence of adsorbed oxygen species on these films can be ruled out on the basis of angle-resolved XPS spectra; the high BE contribution at 530.8 eV in Figure 3ii is likely bulk dissolved oxygen.

It should be noted that, even in the highly oxidized cases shown in Figure 5, the O 1s peak at 528.4 eV is still accompanied by a strong contribution from the peak at 529.0 eV, which is due to Ag_2O. Although the 528.4 eV peak area contribution correlates well with the peak area contribution of the Ag(III) peak and satellite to the overall Ag $3d_{5/2}$ peak, the O 1s peak at 528.4 eV *cannot* represent Ag(III)−O bonding and the peak at 529.0 eV represent Ag(I)−O bonding in AgO. AgO consists of two distinct silver sites but only one oxygen site, with bonding to both Ag(III) and Ag(I); thus, all oxygen anions in AgO are equivalent and should give the same O 1s BE. The presence of 529.0 eV indicates that the highly oxidized film is still mixed phase, likely consisting of AgO, Ag_2O, and potentially Ag_3O_4.

4.5. Why Was Ag(III) Not Observed Previously by XPS? A substantial difference between the present study and the extensive previous work on the silver−oxygen system, which did not observe 366.8 eV as the Ag $3d_{5/2}$ peak for Ag(III), is the very highly oxidizing conditions utilized in the present study. It has been predicted on the basis of oxygen dissociation pressures that AgO would not be stable in vacuum,[22] although it has been shown to be stable in air. Thus, silver oxide powders and films that clearly show the AgO crystal structure by ex situ X-ray diffraction (XRD) may decompose immediately upon introduction into UHV, producing an XPS spectrum of a severely suboxide species (which may still retain the bulk AgO crystal structure[18]). Waterhouse et al.[29] found that higher oxidation compounds are even more unstable. Ag_3O_4 proved too unstable for the collection of XPS spectra, while Ag_2O_3 reportedly decomposes to AgO in less than one hour at room temperature and atmospheric pressure. This instability, combined with the propensity of silver oxides to form highly oxygen deficient substoichiometric compounds, makes it extremely difficult to obtain XPS spectra of highly oxidized silver compounds, whether they are prepared ex situ or in situ. However, depositing very thin films of silver ($\leq$100 Å) in the presence of atomic oxygen and without bulk silver to act as an oxygen sink, and allowing the film to soak in the plasma for long periods of time after deposition, generated a metastable highly oxidized film. Consistent with previous predictions, the highly oxidized film decomposed within days at room temperature in UHV, but its stability in the X-ray beam allowed high resolution XPS spectra to be collected. This may represent the first time that Ag(III) has been obtained in sufficient quantity to be clearly observed by XPS before decomposition.

However, it should be noted that the highly oxidized films prepared in situ in the present study suffer from the same oxide instability as in previous work. Concerns over oxide decomposition with exposure to ambient water, CO_2, and hydrocarbons, as well as the very thin nature of the films ($\leq$100 Å), makes ex situ characterization measurements such as XRD and X-ray absorption impossible, and they were not attempted.

5. Conclusions

Silver oxide thin films with a range of oxidation states were obtained by codeposition of silver metal and atomic oxygen. By depositing thin films without the presence of bulk silver to act as an oxygen sink, highly oxidized films could be formed and studied with high resolution XPS. Under the most oxidizing conditions, an unexpectedly low Ag $3d_{5/2}$ BE of 366.8 eV was observed, with an associated broad satellite at 368.2 eV. On the basis of the known chemistry of silver and the behavior of this species with time and oxidation, it was assigned as low spin Ag(III); the peak position assigned in the literature to Ag(III), 367.3 eV, was assigned to fully oxidized Ag(I). The Ag(III) species was found to be highly unstable in vacuum; by observing decomposition of the oxide over time, quantitative correlations between the Ag $3d_{5/2}$ peak, its associated satellite, and BE and area of the O 1s peak could be made, confirming the silver oxidation state assignment. The theoretical spectrum of high spin Ag(III) was calculated for both an isolated cation and an embedded AgO_6 cluster. The calculated spectra do not match well with experiment, providing strong support to the assignment of low spin Ag(III) in the experimental spectrum. These preliminary results indicate that the failure to adequately determine the Ag/O stoichiometry of the film utilizing accepted XPS sensitivity factors may be due in part to different shake satellite probabilities for O 1s and Ag 3d peaks. Further theoretical work involving material models of low spin systems will aid in the interpretation of the XPS spectra. In addition, further experimental study such as an in situ deposition and oxidation capability, accompanied by in situ XPS, XRD, and X-ray absorption spectroscopy, would make a powerful combination to study the oxidation behavior of silver and draw definitive conclusions regarding oxide phase and charge state.

Acknowledgment. This research was supported by the U.S. Department of Energy (USDOE), Office of Science, Office of Basic Energy Sciences, Division of Materials Sciences and Engineering, and performed using EMSL, a national scientific user facility sponsored by the USDOE's Office of Biological and Environmental Research and located at the Pacific Northwest National Laboratory. P.S.B. acknowledges support from the Geosciences Research Program, Office of Basic Energy Sciences, USDOE. Computer support from the Pittsburgh Supercomputer Center is also acknowledged.

Supporting Information Available: Further details of the electronic structure calculations, Ag MNN spectra of the films shown in Figure 2, and angle-resolved Ag 3d and O 1s XPS spectra of the film shown in Figures 4 and 5. This material is available free of charge via the Internet at http://pubs.acs.org.

References and Notes

(1) Nijhuis, T. A.; Makkee, M.; Moulijn, J. A.; Weckhuysen, B. M. *Ind. Eng. Chem. Res.* **2006**, *45*, 3447.

(2) Van Santen, R. A.; Kuipers, H. P. C. E. The Mechanism of Ethylene Epoxidation. In *Advances in Catalysis*, Eley, D. D., Pines, H., Weisz, P. B., Eds.; Academic Press, Inc.: Orlando, FL, U.S., 1987; Vol. 35.

(3) Wachs, I. E.; Madix, R. J. *Surf. Sci.* **1978**, *76*, 531.

(4) Bao, X.; Muhler, M.; Schedel-Niedrig, T.; Schlogl, R. *Phys. Rev. B* **1996**, *54*, 2249.
(5) Burch, R.; Breen, J. P.; Meunier, F. C. *Appl. Catal. B-Environ.* **2002**, *39*, 283.
(6) Spendelow, J. S.; Wieckowski, A. *Phys. Chem. Chem. Phys.* **2007**, *9*, 2654–2675.
(7) Das, S. S.; Singh, N. P.; Srivastava, P. K. *Prog. Cryst. Growth Charact.* **2009**, *55*, 47–62.
(8) Schnippering, M.; Carrara, M.; Foelske, A.; Kotz, R.; Fermin, D. J. *Phys. Chem. Chem. Phys.* **2007**, *9*, 725–730.
(9) Dellasega, D.; Facibeni, A.; Di Fonzo, F.; Bogana, M.; Polissi, A.; Conti, C.; Ducati, C.; Casari, C. S.; Bassi, A. L.; Bottani, C. E. *Nanotechnology* **2008**, *19*, 475602.
(10) Gao, X. Y.; Wang, S. Y.; Li, J.; Zheng, Y. X.; Zhang, R. J.; Zhou, P.; Yang, Y. M.; Chen, L. Y. *Thin Solid Films* **2004**, *455*, 438–442.
(11) Rivers, S. B.; Bemhardt, G.; Wright, M. W.; Frankel, D. J.; Steeves, M. M.; Lad, R. J. *Thin Solid Films* **2007**, *515*, 8684–8688.
(12) Lu, Z. C.; Gu, Y. J.; Yang, J. X.; Li, Z. S.; Ruan, W. D.; Xu, W. Q.; Zhao, C.; Zhao, B. *Vibr. Spectrosc.* **2008**, *47*, 99–104.
(13) Suzuki, R. O.; Ogawa, T.; Ono, K. *J. Am. Ceram. Soc.* **1999**, *82*, 2033–2038.
(14) Waterhouse, G. I. N.; Bowmaker, G. A.; Metson, J. B. *Appl. Surf. Sci.* **2001**, *183*, 191–204.
(15) Schmidt, A. A.; Offermann, J.; Anton, R. *Thin Solid Films* **1996**, *281−282*, 105.
(16) Li, L.; Yang, J. C.; Minton, T. K. *J. Phys. Chem. C* **2007**, *111*, 6763–6771.
(17) Oakes, D. B.; Krech, R. H.; Upschulte, B. L.; Caledonia, G. E. *J. Appl. Phys.* **1995**, *77*, 2166.
(18) Lutzenkirchen-Hecht, D.; Strehblow, H. H. *Surf. Interface Anal.* **2009**, *41*, 820–829.
(19) Linke, C.; Jansen, M. *Inorg. Chem.* **1994**, *33*, 2614–2616.
(20) Orgel, L. E. *J. Chem. Soc.* **1958**, 4186–4190.
(21) Czyzyk, M. T.; Degroot, R. A.; Dalba, G.; Fornasini, P.; Kisiel, A.; Rocca, F.; Burattini, E. *Phys. Rev. B* **1989**, *39*, 9831–9838.
(22) Tjeng, L. H.; Meinders, M. B. J.; Vanelp, J.; Ghijsen, J.; Sawatzky, G. A.; Johnson, R. L. *Phys. Rev. B* **1990**, *41*, 3190–3199.
(23) Park, K. T.; Novikov, D. L.; Gubanov, V. A.; Freeman, A. J. *Phys. Rev. B* **1994**, *49*, 4425–4431.
(24) Bielmann, M.; Schwaller, P.; Ruffieux, P.; Groning, O.; Schlapbach, L.; Groning, P. *Phys. Rev. B* **2002**, *65*, 235431.
(25) Scatturin, V.; Bellon, P. L. *J. Electrochem. Soc.* **1961**, *108*, 819–822.
(26) Schon, G. *Acta Chem. Scand.* **1973**, *27*, 2623–2633.
(27) Weaver, J. F.; Hoflund, G. B. *Chem. Mater.* **1994**, *6*, 1693–1699.
(28) Weaver, J. F.; Hoflund, G. B. *J. Phys. Chem.* **1994**, *98*, 8519–8524.
(29) Waterhouse, G. I. N.; Metson, J. B.; Bowmaker, G. A. *Polyhedron* **2007**, *26*, 3310–3322.
(30) Xiao, L.; Schneider, W. F. *Chem. Phys. Lett.* **2010**, *484*, 231–236.
(31) Stegelmann, C.; Schiodt, N. C.; Campbell, C. T.; Stoltze, P. *J. Catal.* **2004**, *221*, 630–649.
(32) Hoflund, G. B.; Weaver, J. F.; Epling, W. S. *Surf. Sci. Spectra* **1994−1995**, *3*, 157.
(33) Hoflund, G. B.; Weaver, J. F.; Epling, W. S. *Surf. Sci. Spectra* **1994−1995**, *3*, 163.
(34) Chuang, T. J.; Brundle, C. R.; Rice, D. W. *Surf. Sci.* **1976**, *59*, 413–429.
(35) Bagus, P. S.; Pacchioni, G.; Sousa, C.; Minerva, T.; Parmigiani, F. *Chem. Phys. Lett.* **1992**, *196*, 641–646.
(36) Farhat, E.; Robinkan, S. *Thin Solid Films* **1974**, *23*, 315–322.
(37) Pierson, J. F.; Rousselot, C. *Surf. Coat. Technol.* **2005**, *200*, 276–279.
(38) Hoflund, G. B.; Hazos, Z. F.; Salaita, G. N. *Phys. Rev. B* **2000**, *62*, 11126–11133.
(39) Kaspar, T. C.; Droubay, T.; Chambers, S. A. *Thin Solid Films* **2010**, *519*, 635.
(40) Bagus, P. S.; Broer, R.; de Jong, W. A.; Nieuwpoort, W. C.; Parmigiani, F.; Sangaletti, L. *Phys. Rev. Lett.* **2000**, *84*, 2259–2262.
(41) Bagus, P. S.; Ilton, E. S. *Phys. Rev. B* **2006**, *73*, 155110.
(42) Bagus, P. S.; Nelin, C. J.; Ilton, E. S.; Baron, M.; Abbott, H.; Primorac, E.; Kuhlenbeck, H.; Shaikhutdinov, S.; Freund, H. J. *Chem. Phys. Lett.* **2010**, *487*, 237–240.
(43) Degroot, F. M. F. *J. Electron Spectrosc.* **1994**, *67*, 529–622.
(44) Nelin, C. J.; Bagus, P. S.; Ilton, E. S.; Chambers, S. A.; Kuhlenbeck, H.; Freund, H.-J. *Int. J. Quantum Chem.* **2010**, *110*, 2752.
(45) Chambliss, D. D.; Wilson, R. J. *J. Vac. Sci. Technol. B* **1991**, *9*, 928.
(46) Cercellier, H.; Didiot, C.; Fagot-Revurat, Y.; Kierren, B.; Moreau, L.; Malterre, D.; Reinert, F. *Phys. Rev. B* **2006**, *73*, 195413.
(47) Doniach, S.; Sunjic, M. *J. Phys. C* **1970**, *3*, 285.
(48) Moulder, J. F.; Stickle, W. F.; Sobol, P. E.; Bomben, K. D. *Handbook of X-ray Photoelectron Spectroscopy*; Perkin-Elmer Corp.: Eden Prairie, MN, U.S., 1992.
(49) Czanderna, A. W. *J. Phys. Chem.* **1964**, *68*, 2765.
(50) Cotton, F. A.; Wilkinson, G. *Basic Inorganic Chemistry*; John Wiley and Sons, Inc.: New York, NY, U.S., 1976.
(51) Bagus, P. S.; Illas, F.; Pacchioni, G.; Parmigiani, F. *J. Electron Spectrosc.* **1999**, *100*, 215–236.
(52) Bagus, P. S.; Ilton, E. S.; Rustad, J. R. *Phys. Rev. B* **2004**, *69*, 205112.
(53) Scofield, J. H. *J. Electron Spectros.* **1976**, *8*, 129–137.
(54) Yeh, J. J.; Lindau, I. *Atom. Data Nucl. Data* **1985**, *32*, 1–155.
(55) Wagner, C. D.; Davis, L. E.; Zeller, M. V.; Taylor, J. A.; Raymond, R. H.; Gale, L. H. *Surf. Interface Anal.* **1981**, *3*, 211.

JP107914E